Harnessing microbial subsurface metal reduction activities to synthesise nanoscale cobalt ferrite with enhanced magnetic properties

Victoria S. Coker[1*], Neil D. Telling[1], Gerrit van der Laan[3,1], Richard A.D. Pattrick[1], Carolyn I. Pearce[1], Elke Arenholz[4], Floriana Tuna[2], Richard Winpenny[2] and Jonathan R. Lloyd[1]

[1]School of Earth, Atmospheric and Environmental Sciences and Williamson Research Centre for Molecular Environmental Science, University of Manchester, Manchester, M13 9PL, UK

[2]School of Chemistry, University of Manchester, Manchester, M13 9PL, UK

[3]Diamond Light Source, Didcot, Oxfordshire, OX11 0DE, UK

[4]Advanced Light Source, Lawrence Berkeley National Laboratory, Berkeley, CA 94720, USA

*vicky.coker@manchester.ac.uk

Abstract

Nanoscale ferrimagnetic particles have a diverse range of uses from directed cancer therapy and drug delivery systems to magnetic recording media and transducers. Such applications require the production of monodisperse nanoparticles with well-controlled size, composition, and magnetic properties. To fabricate these materials purely using synthetic methods is costly in both environmental and economical terms. However, metal-reducing microorganisms offer an untapped resource to produce these materials. Here, the Fe(III)-reducing bacterium Geobacter sulfurreducens is used to synthesize magnetic iron oxide nanoparticles. A combination of electron microscopy, soft X-ray spectroscopy, and magnetometry techniques was employed to show that this method of biosynthesis results in high yields of crystalline nanoparticles with a narrow size distribution and magnetic properties equal to the best chemically synthesized materials. In particular, it is demonstrated here that cobalt ferrite ($CoFe_2O_4$) nanoparticles with low

temperature coercivity approaching 8 kOe and an effective anisotropy constant of ~10^6 erg cm^{-3} can be manufactured through this biotechnological route. The dramatic enhancement in the magnetic properties of the nanoparticles by the introduction of high quantities of Co into the spinel structure represents a significant advance over previous biomineralization studies in this area using magnetotactic bacteria. The successful production of nanoparticulate ferrites achieved in this study at high yields could open up the way for the scaled-up industrial manufacture of nanoparticles using environmentally benign methodologies.

The production of ferromagnetic nanoparticles for pioneering cancer therapy, drug delivery, chemical sensors, catalytic activity, photoconductive materials, as well as more traditional uses in data storage embodies a large area of inorganic synthesis research.(1-4) In particular, the addition of transition metals other than Fe into the structure of magnetite (Fe_3O_4) has been shown to greatly enhance the magnetic properties of the particles, tailoring them to different commercial uses.(1, 2, 5) However, synthesis of magnetic nanoparticles is often carried out at high temperatures with toxic solvents resulting in high environmental and energy costs. Additionally, these ferrite nanoparticles are not intrinsically biocompatible, and to make them suitable for insertion into the human body is a rather intricate task.

A relatively unexplored resource for magnetic nanomaterial production is subsurface Fe(III)-reducing bacteria, as these microorganisms are capable of producing large quantities of nanoscale magnetite (Fe_3O_4) at ambient temperatures. Metal-reducing bacteria live in environments deficient in oxygen and conserve energy for growth through the oxidation of hydrogen or organic electron donors, coupled to the reduction of oxidized metals such as Fe(III)-bearing minerals.(6) This can result in the formation of magnetite *via* the extracellular reduction of amorphous Fe(III)-oxyhydroxides causing the release of soluble Fe(II) and resulting in complete recrystallization of the amorphous mineral into a new phase.(7, 8) Some previous studies have reported altering the

composition of biogenic magnetite produced by Fe(III)-reducing bacteria for industrial and environmental applications.(9, 10) However, research into the commercial exploitation of bacteria to form magnetic minerals has focused primarily on magnetotactic bacteria which form magnetosomal magnetite internally using very different pathways to those bacteria forming magnetite outside the cell.(11-14) Magnetotactic bacteria live at the sediment−water interface and use internal nanomagnets to guide them to their preferred environmental niche using the Earth's magnetic field. Since magnetotactic bacteria generally grow optimally under carefully controlled microaerobic conditions, the culturing processes for these organisms are challenging and result in low yields of nanomagnetite. Despite these limitations, magnetotactic bacteria have been shown to incorporate ~1% Co into the magnetite structure *in vivo*,(15) and $CoFe_2O_4$ was synthesized *in vitro*,(14) altering the magnetic properties of the material formed. Although these previous studies are an important first step, in order to obtain the degree of control over the magnetic properties required by potential applications, Co must be incorporated into the spinel structure together with high nanoparticle yields. It is not clear at present how this could be achieved using the highly regulated intracellular magnetosome systems.

Here we present an alternative and efficient method to produce large quantities of highly crystalline magnetite and cobalt ferrite nanoparticles using the Fe(III)-reducing bacterium, Geobacter sulfurreducens, at ambient temperatures through the extracellular dissimilatory reduction of Fe(III)-oxyhydroxides without and with addition of cobalt. A suite of three samples containing progressive additions of Co was produced for this study. A combination of transmission electron microscopy (TEM), X-ray diffraction (XRD), X-ray absorption (XA), and X-ray magnetic circular dichroism (XMCD) was used to determine the crystallographic structure, site occupancies, and valence states of the Fe and Co cations within the spinel structure. Furthermore, superconducting quantum interference device (SQUID) magnetometry was used to determine the magnetic properties of these materials. The exceptional ability of the bacteria to manufacture a wide range of useful nanomaterials has until now been overlooked for production on a commercial scale.

Results and discussion

Biogenic magnetite and two related materials (biogenic Co-ferrite-1 and biogenic Co-ferrite-2) were produced from starting materials of Fe(III)-oxyhydroxide containing increasing amounts of co-precipitated Co(II), at ambient temperature and pressure using the metal-reducing bacterium Geobacter sulfurreducens. Conversion of the amorphous Fe(III)-oxyhydroxide occurred during the reductive transformation by G. sulfurreducens to give a biomineral phase enriched with Fe(II), while control experiments without cells showed no change in acid-extractable Fe(II) (see Supporting Information). The yield of nanoparticles in this experiment was 1.6 g per 100 mL per day, which is comparable to or greater than yields given by other bacterial synthesis methods.(14, 16) Energy dispersive X-ray (EDX) analysis of the particles indicated that the Co content of the total cation distribution was 6 atom % for Co-ferrite-1 and 23 atom % for Co-ferrite-2. The latter is close to the Co content of stoichiometric Co-ferrite ($CoFe_2O_4$). X-ray diffraction (XRD) and selected area electron diffraction (SAED) in Figure 1 show that each of the samples gives only reflections arising from a ferrite structure. Interestingly, it was found that the particle size decreases for increasing Co content, as revealed by an overall broadening of the individual diffraction peaks in Figure 1a. Fitting the (311) diffraction peak with a Lorentzian line shape using the Scherrer equation(17) gives the crystallite size for each material (Table 1). The XRD shows that the material is nanocrystalline, where the addition of 23 atom % Co into the structure reduces the average crystallite size from 15−16 to 8 nm. These values correlate well with the observed particle sizes in TEM images (Figure 1), confirming the single crystalline nature. In addition, the TEM images—as well as magnetization measurements discussed below—indicate a narrow size distribution of the particles, crucially important for many technological applications.

The cation distribution in the ferrite nanoparticles was investigated using X-ray magnetic circular dichroism (XMCD) at the Fe $L_{2,3}$ and Co $L_{2,3}$ X-ray absorption edges. XMCD is the difference in the absorption of circularly polarized X-rays for opposite sample magnetization directions. Stoichiometric magnetite is an inverse spinel, which contains tetrahedral (T_d) and octahedral [O_h] sites accommodating Fe^{2+} and Fe^{3+} cations according

to the formula $(Fe^{3+})_{Td}[Fe^{2+}Fe^{3+}]_{Oh}O_4$. Each specific cation in the spinel structure generates a unique XMCD signature that is determined by its valence state (number of *d* electrons), site symmetry (*i.e.*, T_d or O_h), and magnetization (local moment) direction. The XA and XMCD spectra of the individual cations can be computed using atomic multiplet calculations.(18, 19) By fitting a weighted sum of these calculated spectra to the measured XMCD, the site distribution of the Fe cations can be obtained (for details see ref 20). Figure 2a shows the data together with the calculated fits for the Fe $L_{2,3}$ spectra of the biomagnetite and Co-enriched bioferrite samples. Figure 2b gives the relative proportions of the three Fe components, Fe^{2+} O_h, Fe^{3+} T_d, and Fe^{3+} O_h, which primarily make up the intensities of the three main peaks (negative, positive, and negative, respectively) in the Fe L_3 edge (~708−714 eV). A comparison of the biogenic materials shows that the most striking change with increasing Co amount is the gradual decrease in intensity of the leading negative peak in the Fe L_3 edge, corresponding to a decrease in Fe^{2+} O_h content. The best-fit spectra give the values for the relative site occupancies as indicated in Figure 2b. The Fe^{2+}/Fe^{3+} ratio in biogenic magnetite is 1.22:2, which is higher than the 1:2 ratio expected for stoichiometric magnetite, which is due to an increased amount of Fe d^6 O_h as a result of the anoxic environment in which the magnetite was formed.(20, 21) Upon the addition of Co, the amount of Fe^{2+} decreases rapidly, with only a small accompanying change in the amount of Fe^{3+} cations per formula unit. This implies that Co is predominantly replacing Fe^{2+} cations in octahedral sites.

The site occupancy and oxidation state of the Co can be directly assessed by examining the Co $L_{2,3}$ XA and XMCD spectra (Figure 3). The close similarity between the spectra for Co-ferrite-2 and synthetically produced $CoFe_2O_4$ thin films(22) signifies that the bacteria were able to suitably accommodate Co in the ferrite structure. Calculated XA and XMCD spectra for Co^{2+} (Figure 3b) and Co^{3+} (Figure 3c) in both O_h and T_d coordination have been normalized and broadened to account for instrumental broadening for comparison with experimental spectra (Figure 3a). The strong resemblance of the experimental data to the calculated Co^{2+} O_h XA and XMCD suggests that the Co cations reside primarily on these sites, particularly as the magnetic moments on the T_d and O_h

sites are antiferromagnetically coupled, resulting in an XMCD with opposite sign for the two sites. The measurements show that the sign of the Co XMCD is the same as that of the Fe O_h XMCD, hence confirming the O_h site occupancy of Co. Further confirmation arises from the fact that the presence of the Co^{2+} O_h coincides directly with the decrease in Fe^{2+} on octahedral sites found from the Fe $L_{2,3}$ XMCD. Nevertheless, a small amount (~10%) of Co residing in a different site or as Co^{3+} cannot be discounted as the fit is not perfect, particularly at the high energy side of the L_3.

The magnetic properties of the nanoparticles, graphically represented in Figure 4, are governed by the anisotropy energy, which constrains the nanoparticle magnetization to align along a specific direction known as the easy axis. The maximum anisotropy energy for a particular nanoparticle depends on the product of its volume, V, and anisotropy constant, K. Above the so-called blocking temperature, T_B, the thermal energy is sufficient to surmount the anisotropy energy barrier and the nanoparticle magnetization is free to align in arbitrary directions. Thus, for an assembly of such nanoparticles, the net magnetization measured in the absence of an applied magnetic field (*i.e.*, the remanent magnetization of the sample) will average out to zero and the particles are said to be in superparamagnetic state.

MethodsSynthetic amorphous Fe(III)-oxyhydroxide was produced using the method of Lovley and Philips,(37) where a 0.4 mol solution of $FeCl_3$ is neutralized by 10 N NaOH to pH 7 and the solid then washed in deionized H_2O until no Cl^- ions remain. $CoCl_2 \cdot 6H_2O$ was added prior to neutralization at a concentration of either 0.02 or 0.132 mol to create FeCo-oxyhydroxides which formed a suite of starting materials with an increasing amount of cobalt which result in samples Co-ferrite-1 and Co-ferrite-2, respectively. The starting material was characterized using XRD to confirm that poorly crystalline material had formed. Geobacter sulfurreducens was obtained from our laboratory culture collection at the Williamson Centre for Molecular Environmental Science at the University of Manchester and grown under strictly anaerobic conditions at 30 °C in modified fresh water medium.(38) Sodium acetate (20 mmol) and fumarate (40 mmol) were provided as the electron donor and acceptor, respectively. All manipulations

were done under an atmosphere of N_2−CO_2 (80:20). Late log-phase cultures of G. sulfurreducens were harvested by centrifugation at 4920*g* for 20 min and washed twice in bicarbonate buffer ($NaHCO_3$ 30 mmol, pH 7.1) under N_2−CO_2 (80:20) gas prior to use. Aliquots of the washed cell suspension (1.5 mL) were added to sealed anaerobic bottles containing 28.5 mL of bicarbonate buffer to a final concentration of bacteria of ~0.2 mg protein per mL. The following additions were made from anaerobic stocks as required: an Fe(III)-oxyhydroxide or CoFe(III)-oxyhydroxide suspension (10 mmol L^{-1}), sodium acetate (10 mmol), and anthraquinone 2,6-disulfonate (10 μmol). Bottles were incubated in the dark at 20 °C; 100 μL of slurry was removed from each serum bottle periodically, using aseptic and anaerobic technique and analyzed for 0.5 mol HCl-extractable Fe^{2+} employing the ferrozine method.(37) After ferrite formation, samples were washed twice in deionized water to remove cells and buffer solution. Aliquots of the sample suspension were then dropped on carbon-coated copper grids and left to dry prior to introduction into the microscope.

Transmission electron microscopy (TEM) was carried out using a Phillips/FEI Tecnai electron microscope equipped with a field emission gun (FEG), EDX system (Oxford Instruments UTW ISIS), and Gatan imaging filter (GIF). All TEM images presented here are bright-field images obtained using an operating beam voltage of 300 keV. Selected area electron diffraction (SAED) patterns were acquired using an appropriate diffraction aperture. All (powder) X-ray diffraction (XRD) measurements were acquired over a 2θ range of 10−70° with a step size of 0.02° using a Bruker D8Advance with Cu $K\alpha_1$ source. X-ray absorption (XA) spectra at the Fe and Co $L_{2,3}$ edges were obtained on beamline 4.0.2 at the Advanced Light Source (ALS), Berkeley, CA, using the eight-pole resistive magnet endstation.(39) Samples were prepared by washing aliquots of the suspension in deionized water before drying under anaerobic conditions. The powders were then, in an anaerobic cabinet, mounted on carbon tape attached to the sample manipulator. XA was monitored in total-electron yield (TEY) mode, which has an effective probing depth of ~ 4.5 nm. At each photon energy of the spectrum, the XA was measured for two opposite magnetization directions by reversing the applied field of 0.6 T. After normalization to the incident beam intensity, the XMCD is obtained as the difference between the two XA spectra.(40) To obtain the cation distribution over the three Fe sites, the experimental

XMCD was fitted by means of a nonlinear least-squares analysis, using the calculated spectra for each site. In these calculations, described in refs 18 and 19, the 10Dq crystal field parameters were taken as 1.2 and −0.6 eV for Fe O_h and T_d sites and 0.9 and −0.5 eV for Co O_h and T_d sites. The results were convoluted by a Lorentzian of $\Gamma = 0.3$ (0.5) eV for the L_3 (L_2) edge to account for intrinsic core-hole lifetime broadening and by a Gaussian of $\sigma = 0.2$ eV to account for instrumental broadening.

Magnetic measurements were performed on polycrystalline samples restrained in eicosane, using a Quantum Design MPMS-XL SQUID magnetometer equipped with a 7 T magnet. Zero-field cooled (ZFC) and field-cooled (FC) magnetization curves were recorded over 5−300 K temperature range with an applied magnetic field of 100 Oe. The diamagnetism of the sample holder and of eicosane was measured and extracted from the raw magnetic data.

Acknowledgment

This work was supported by the EPSRC grants EPSRC EP/D057310/1 and EP/D058767/1 and BBSRC grant BB/E003788/1. We would like to thank E. McInnes for assistance with SQUID measurements, G. Cliff for TEM support, and J. Waters for XRD support. The Advanced Light Source is supported by the Director, Office of Science, Office of Basic Energy Sciences, of the U.S. Department of Energy under Contract No. DE-AC02-05CH11231.

References

1. Ritter, J. A.; Ebner, A. D.; Daniel, K. D.; Stewart, K. L.
   Application of High Gradient Magnetic Separation Principles to Magnetic Drug Targeting
   J. Magn. Magn. Mater. 2004, 280, 184–201

2. Kim, D.-H.; Nikles, D. E.; Johnson, D. T.; Brazel, C. S.
   Heat Generation of Aqueously Dispersed $CoFe_2O_4$ Nanoparticles as Heating Agents for Magnetically Activated Drug Delivery and Hyperthermia
   J. Magn. Magn. Mater. 2008, 320, 2390–2396

3. Safarik, I.; Safarikova, M.
   Magnetic Nanoparticles and Biosciences
   Monatsh. Chem. 2002, 133, 737–759

4. Jolivet, J.-P.; Tronc, E.; Chaneac, C.
   Synthesis of Iron Oxide-Based Magnetic Nanomaterials and Composites
   C. R. Chim. 2002, 5, 659–664

5. Sun, S.; Zeng, H.; Robinson, D. B.; Raoux, S.; Rice, P. M.; Wang, S. X.; Li, G.
   Monodisperse MFe_2O_4 (M = Fe, Co, Mn) Nanoparticles
   J. Am. Chem. Soc. 2004, 126, 273–279

6. Caccavo, F., Jr.; Lonergan, D. J.; Lovley, D. R.; Davis, M.; Stolz, J. F.; McInerney, M. J. Geobacter sulfurreducens, sp. nov., a Hydrogen and Acetate-Oxidising Dissimilatory Metal Reducing Bacterium Appl. Environ. Microbiol. 1994, 60, 3752–3759

7. Coker, V. S.; Bell, A. M. T.; Pearce, C. I.; Pattrick, R. A. D.; van der Laan, G.; Lloyd, J. R.
   Time-Resolved Synchrotron X-ray Powder Diffraction Study of Magnetite Formation by the Fe(III)-Reducing Bacterium Geobacter sulfurreducens
   Am. Mineral. 2008, 93, 540–547

8. Hansel, C. M.; Benner, S. G.; Neiss, J.; Dohnalkova, A.; Kukkadapu, R. K.; Fendorf, S. Secondary
Mineralization Pathways Induced by Dissimilatory Iron Reduction of Ferrihydrite under Advective Flow
Geochim. Cosmochim. Acta 2003, 67, 2977–2992

9. Fredrickson, J. K.; Zachara, J. M.; Kukkadapu, R. K.; Gorby, Y. A.; Smith, S. C.; Brown, C. F.
Biotransformation of Ni-Substituted Hydrous Ferric Oxide by an Fe(III)-Reducing Bacterium
Environ. Sci. Technol. 2001, 35, 703–712

10. Moon, J.-W.; Yeary, L. W.; Rondinone, A. J.; Rawn, C. J.; Kirkham, M. J.; Roh, Y.; Love, L. J.; Phelps, T. J.
Magnetic Response of Microbially Synthesized Transition Metal- and Lanthanide-Substituted Nanosized Magnetites
J. Magn. Magn. Mater. 2007, 313, 283–292

11. Matsunaga, T.; Okamura, Y.; Tanaka, T.
Biotechnological Applications of Nano-Scale Engineered Bacterial Magnetic Particles
J. Mater. Chem. 2004, 14, 2099–2105

12. Lang, C.; Schuler, D.
Biogenic Nanoparticles: Production, Characterization, and Application of Bacterial Magnetosomes
J. Phys.: Condens. Mater. 2006, 18, S2815–S2828

13. Matsunaga, T.; Suzuki, Y.; Tanaka, M.; Arakaki, A.
Molecular Analysis of Magnetotactic Bacteria and Development of Functional Bacterial Magnetic Particles for Nano-Biotechnology
Trends Biotechnol. 2007, 25, 182–188

14. Prozorov, T.; Palo, P.; Wang, L.; Nilsen-Hamilton, M.; Jones, D.; Orr, D.; Mallapragada, S. K.; Narasimhan, B.; Canfield, P. C.; Prozorov, R.

15. Staniland, S.; Williams, W.; Telling, N. D.; van der Laan, G.; Harrison, A.; Ward, B.
Controlled Cobalt Doping of Magnetosomes *In Vivo*
Nat. Nanotechnol. 2008, 3, 158–162

16. Roh, Y.; Vali, H.; Phelps, T. J.; Moon, J.-W.
Extracellular Synthesis of Magnetite and Metal-Substituted Magnetite Nanoparticles
J. Nanosci.
Nanotechnol. 2006, 6, 3517–3520

17. Scherrer, P.
Estimation of Size and Internal Structure of Colloidal Particles by Means of Rontgen Rays
Nachr. Ges. Wiss. Goettingen 1918, 96–100

18. van der Laan, G.; Kirkman, I. W.
The 2*p* Absorption Spectra of 3*d* Transition Metal Compounds in Tetrahedral and Octahedral Symmetry
J. Phys.: Condens. Mater. 1992, 4, 4189–4204

19. van der Laan, G.; Thole, B. T.
Strong Magnetic X-ray Dichroism in 2*p* Absorption Spectra of 3*d* Transition Metal Ions
Phys. Rev. B 1991, 43, 13401–13411

20. Coker, V. S.; Pearce, C. I.; Lang, C.; van der Laan, G.; Pattrick, R. A. D.; Telling, N. D.; Schuler, D.; Arenholz, E.; Lloyd, J. R.
Cation Site Occupancy of Biogenic Magnetite Compared to Polygenic Ferrite Spinels Determined by X-ray Magnetic Circular Dichroism
Eur. J. Mineral. 2007, 19, 707–716

21. Carvallo, C.; Sainctavit, P.; Arrio, M.-A.; Menguy, N.; Wang, Y.; Ona-Nguema, G.; Brice-Profeta, S.

Biogenic *vs.* Abiogenic Magnetite Nanoparticles: A XMCD Study
Am. Mineral. 2008, 93, 880–885

22. van der Laan, G.; Arenholz, E.; Chopdekar, R. V.; Suzuki, Y.
Influence of Crystal Field on Anisotropic X-ray Magnetic Linear Dichroism at the Co^{2+} $L_{2,3}$ Edges
Phys. Rev. B 2008, 77, 064407-1/11

23. Zhang, X. X.; Hernandez, J. M.; Tejada, J.; Ziolo, R. F.
Magnetic Properties, Relaxation, and Quantum Tunneling in $CoFe_2O_4$ Nanoparticles Embedded in Potassium Silicate
Phys. Rev. B 1996, 54, 4101–4106

24. Verwey, E. J. W.
Electronic Conduction in Magnetite (Fe_3O_4) and its Transition Point at Low Temperatures
Nature 1939, 144, 327–328

25. Goya, G. F.; Berquo, T. S.; Fonseca, F. C.; Morales, M. P.
Static and Dynamic Magnetic Properties of Spherical Magnetite Nanoparticles
J. Appl. Phys. 2003, 94, 3520–3528

26. Brabers, V. A. M.; Walz, F.; Kronmuller, H.
Impurity Effects Upon the Verwey Transition in Magnetite
Phys. Rev. B 1998, 58, 14163–14166

27. Bean, C. P.
Hysteresis Loops of Mixtures of Ferromagnetic Micropowders
J. Appl. Phys. 1955, 26, 1381–1383

28. Granqvist, C. G.; Buhrman, R. A.
Ultrafine Metal Particles
J. Appl. Phys. 1976, 47, 2200–2219

29. von Helmolt, R.; Wecker, J.; Samwer, K. Calculation of Particle Size from Magnetization and Resistance Curves in Giant Magnetoresistive Heterogeneous

30. Fortin, J.-P.; Wilhelm, C.; Servais, J.; Menager, C.; Bacri, J.-C.; Gazeau, F.
Size-Sorted Anionic Iron Oxide Nanomagnets as Colloidal Mediators for Magnetic Hyperthermia J. Am. Chem. Soc. 2007, 129, 2628–2635

31. Chikazumi, S.
The Physics of Ferromagnetism, 2nd ed.;
Oxford University Press: Oxford, 1997.

32. Ibusuki, T.; Kojima, S.; Kitakami, O.; Shimada, Y.
Magnetic Anisotropy and Behaviours of Fe Nanoparticles
IEEE Trans. Magn. 2001, 37, 2223–2225

33. Lopez, J. L.; Pfannes, H.-D.; Paniago, R.; Sinnecker, J. P.; Novak, M. A.
Investigation of the Static and Dynamic Magnetic Properties of $CoFe_2O_4$ Nanoparticles
J. Magn. Magn. Mater. 2008, 320, e327–e330

34. Rosensweig, R. E.
Heating Magnetic Fluid with Alternating Magnetic Field
J. Magn. Magn. Mater. 2002, 252, 370–374

35. Craik, D. J.
Intrinsic and Technical Magnetic Properties of Oxides. In Magnetic Oxides;
Craik, D. J. , Ed.; Wiley: London, 1975; pp 1−96.

36. Coey, J. M. D.
Noncollinear Spin Arrangement in Ultrafine Ferromagnetic Crystallites
Phys. Rev. Lett. 1971, 27, 1140–1142

37. Lovley, D. R.; Phillips, E. J. P.
Availability of Ferric Iron for Microbial Reduction in Bottom Sediments of the Freshwater Tidal Potomac River
Appl. Environ. Microbiol. 1986, 52, 751–757

38. Lloyd, J. R.; Leang, C.; Hodges Myerson, A. L.; Coppi, M. V.; Cuifo, S.; Methe, B.; Sandler, S. J.; Lovley, D. R.
Biochemical and Genetic Characterization of PpcA, a Periplasmic *c*-type Cytochrome in Geobacter sulfurreducens
Biochem. J. 2003, 369, 153–161

39. Arenholz, E.; Prestemon, S. O.
Design and Performance of an Eight-Pole Resistive Magnet for Soft X-ray Magnetic Dichroism Measurements
Rev. Sci. Instrum. 2005, 76, 083908/1-8

40. Pattrick, R. A. D.; van der Laan, G.; Henderson, C. M. B.; Kuiper, P.; Dudzik, E.; Vaughan, D. J.
Cation Site Occupancy in Spinel Ferrites Studied by X-ray Magnetic Circular Dichroism: Developing a Method for Mineralogists
Eur. J. Mineral. 2002, 14, 1095–1102

Figure Legends

Table 1. Structural and Magnetic Properties from Biogenic Magnetite and Co-Enriched Bioferrites

Figure 1. (a) X-ray diffraction of biogenic magnetite, Co-ferrite-1, and Co-ferrite-2. Transmission electron microscopy (TEM) with selected area diffraction (inset) for biogenic (b) magnetite and (c) Co-ferrite-2. Note the different scale bars of the TEM images.

Figure 2. (a) Experimental Fe $L_{2,3}$ XMCD spectra (black circles) with best-fit spectra (red line) for biogenic (i) magnetite, (ii) Co-ferrite-1, and (iii) Co-ferrite-2. (b) For the best-fit spectrum of each biogenic sample, the decomposition into the spectra for the Fe^{2+} O_h, Fe^{3+} T_d, and Fe^{3+} O_h components is given. The color-coded numbers indicate the proportions of the components, and the error bar for each site occupancy is ±0.02 cations.]

Figure 3. (a) Experimental Co $L_{2,3}$ XA and XMCD spectra for biogenic Co-ferrite-2. Calculated XA and XMCD spectra for (b) Co^{2+} and (c) Co^{3+} in octahedral (red line) tetrahedral (blue line) coordination. Calculations were done following the method of refs 18 and 19.

Figure 4. SQUID magnetometry measurements. (a) Zero-field cooled (ZFC) and field cooled (FC) curves for biogenic magnetite (red lines) and biogenic Co-ferrite-2 (blues lines). (b) Magnetic hysteresis curve at 273 K for Co-ferrite-2 with Langevin function fitting and (inset) derived particle size distribution. (c) Fit for biogenic magnetite using the Law of Approach to Saturation. (d) Magnetic hysteresis curves taken at 5 K for biogenic magnetite (red line) and Co-ferrite-2 (blue line).

Table 1.

sample	**biomagnetite**	**Co-ferrite-1**	**Co-ferrite-2**
EDX Co/Fe ratio	0.00:1	0.06:1	0.30:1
XRD crystallite size (nm)	15	16	8
saturation magnetization, M_S (emu g^{-1}) at 298 K	78	–	48
remanent magnetization, M_R/M_S at 298 K/at 5 K	0.06/0.25	–	0.04/0.62
coercivity, H_C (Oe) at 5 K	360	–	7900
median particle diameter, d_0 (nm)	–	–	7.9
most probable diameter, d_p (nm)	–	–	6.8
dispersion index, σ_d	–	–	0.38

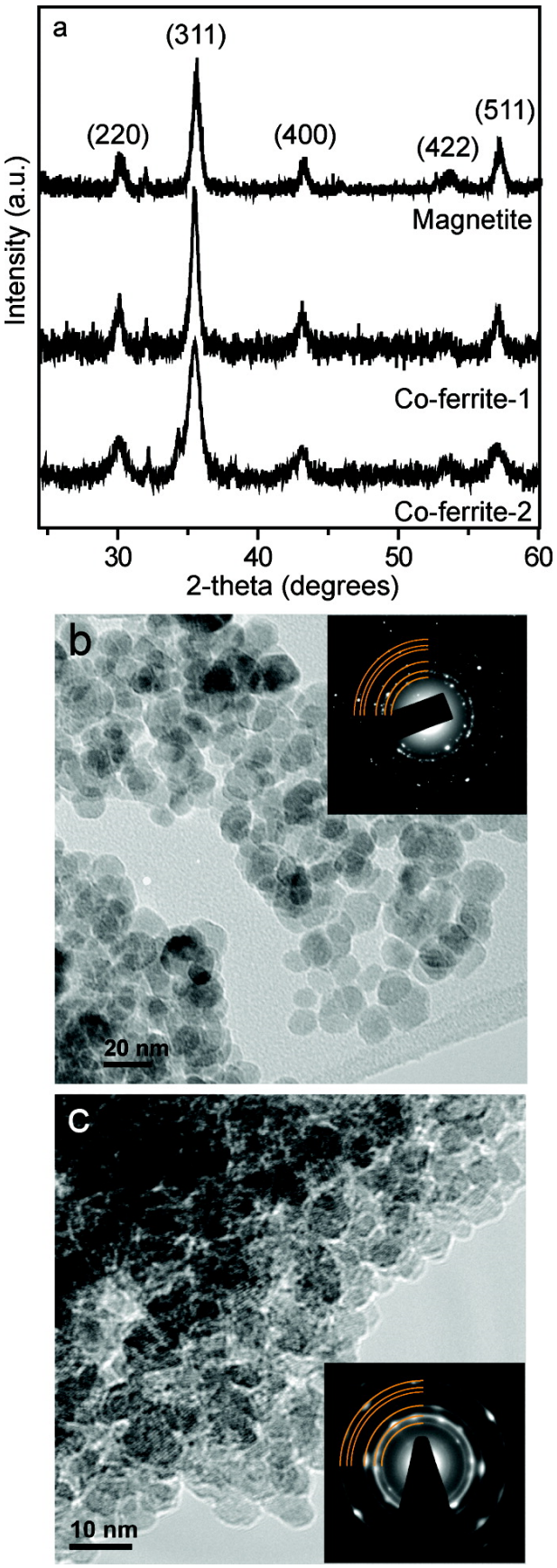
a
(311)
(220)
(400)
(422)
(511)
Magnetite
Co-ferrite-1
Co-ferrite-2
Intensity (a.u.)
30
40
50
60
2-theta (degrees)
b
20 nm
c
10 nm

Figure 1

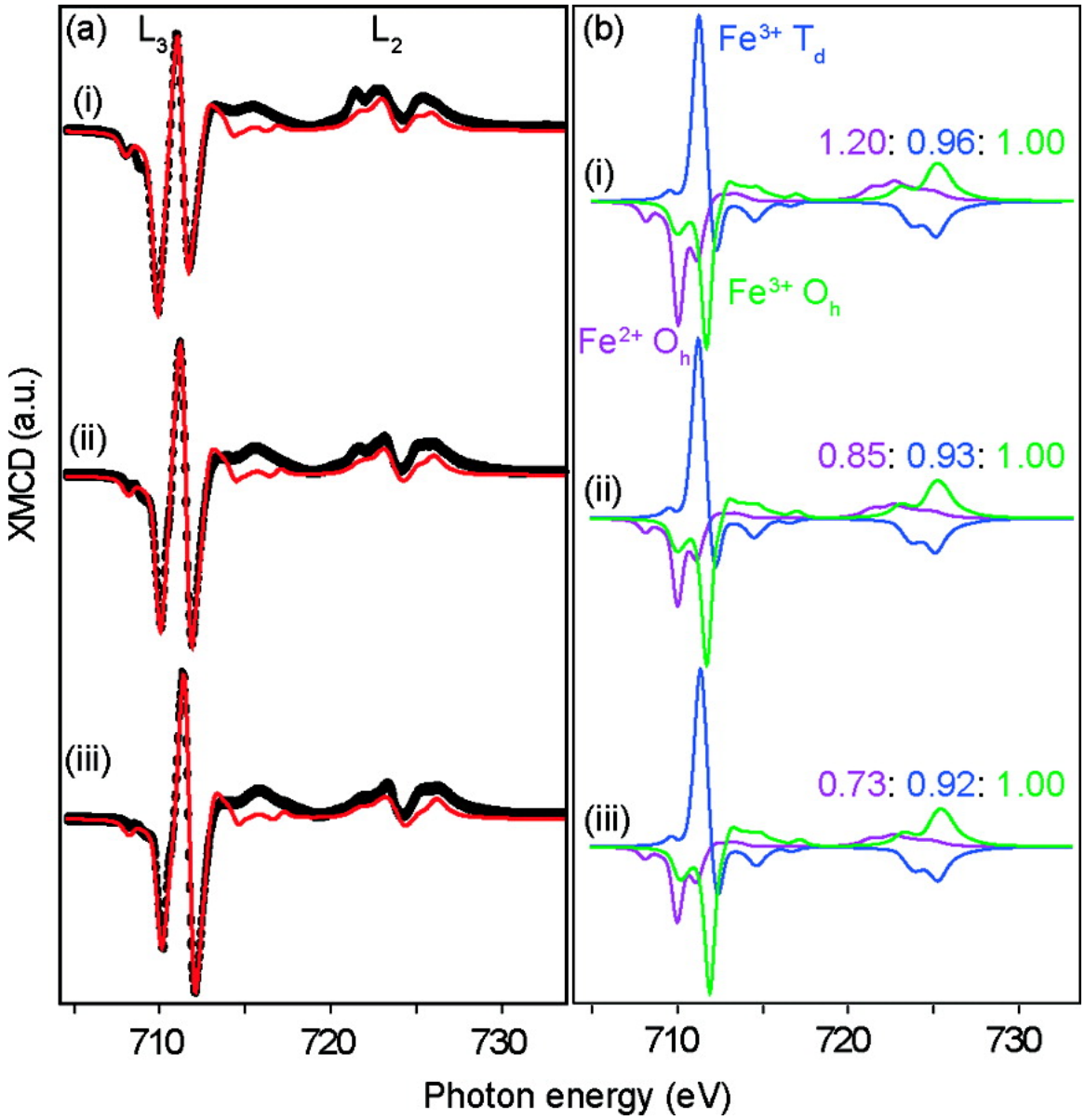
(a)
L3
L2
(i)
(ii)
(iii)
XMCD (a.u.)
(b)
Fe3+ Td
1.20: 0.96: 1.00
(i)
Fe3+ Oh
Fe2+ Oh
0.85: 0.93: 1.00
(ii)
0.73: 0.92: 1.00
(iii)
710
720
730
710
720
730
Photon energy (eV)

Figure 2

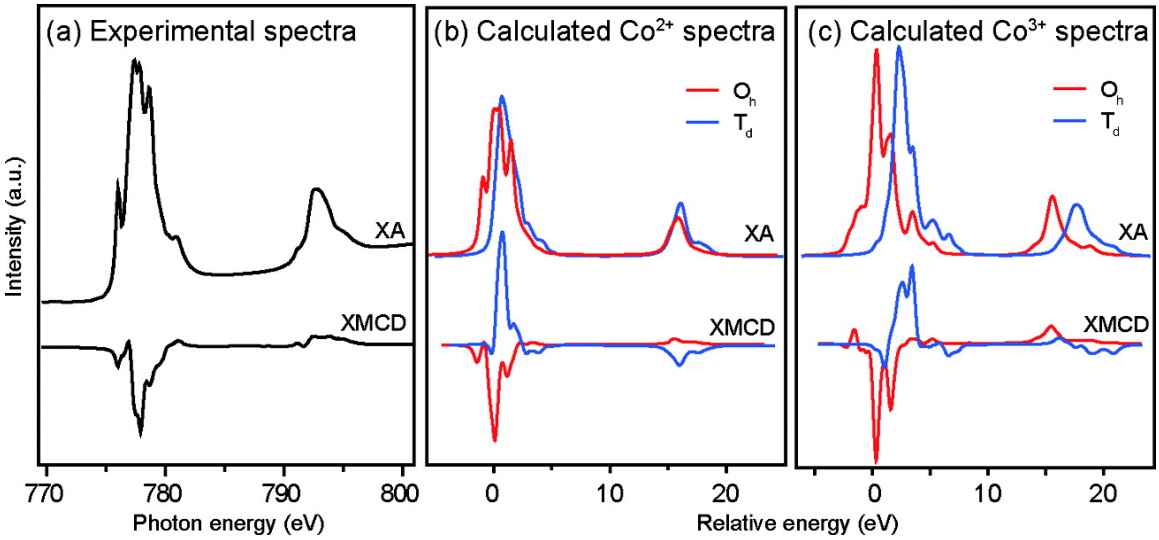
(a) Experimental spectra
(b) Calculated Co2+ spectra
(c) Calculated Co3+ spectra
Intensity (a.u.)
XA
XMCD
Oh
Td
770
780
790
800
0
10
20
Photon energy (eV)
Relative energy (eV)

Figure 3

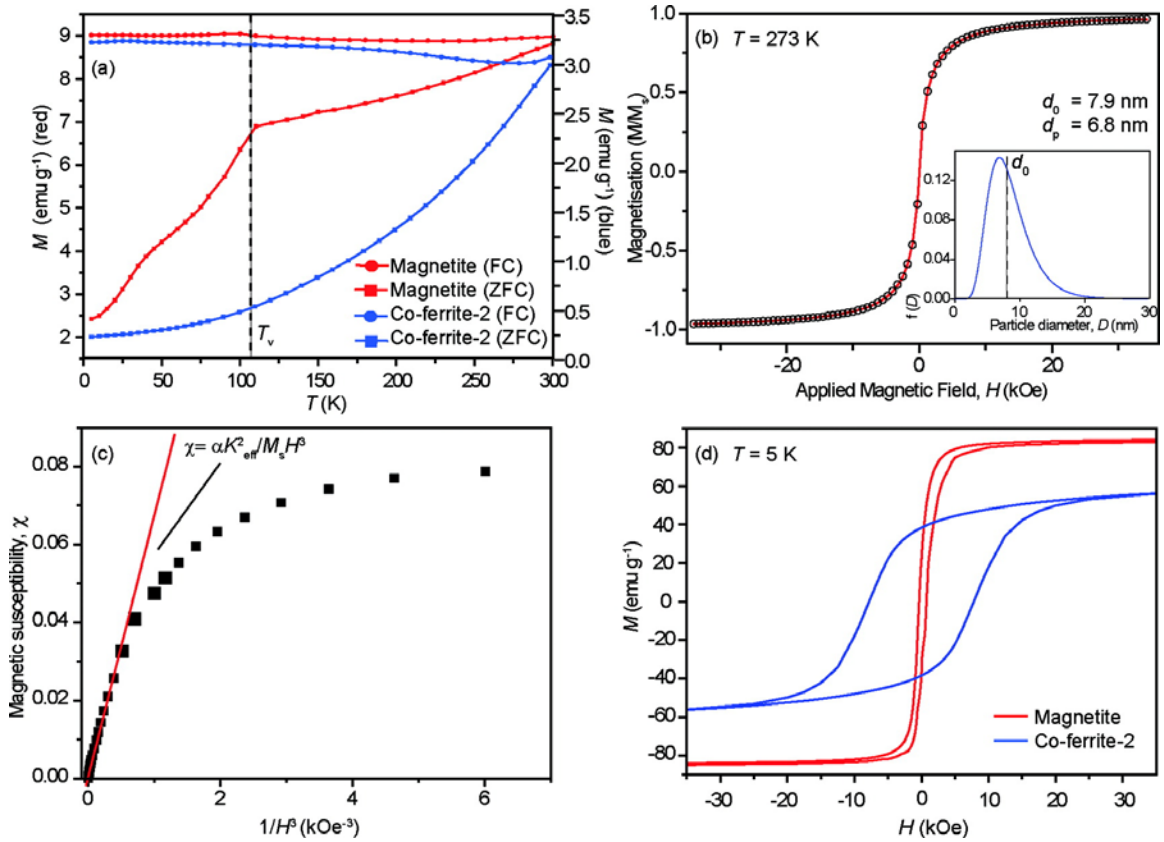
(a)
M (emu g-1) (red)
M (emu g-1) (blue)
T (K)
Tv
Magnetite (FC)
Magnetite (ZFC)
Co-ferrite-2 (FC)
Co-ferrite-2 (ZFC)
(b) T = 273 K
d0 = 7.9 nm
dp = 6.8 nm
d0
f (D)
Particle diameter, D (nm)
Magnetisation (M/Ms)
Applied Magnetic Field, H (kOe)
(c)
χ= αK2eff/MsH3
Magnetic susceptibility, χ
1/H3 (kOe-3)
(d) T = 5 K
M (emu g-1)
Magnetite
Co-ferrite-2
H (kOe)

Figure 4